SECTION 4

EARTHQUAKE SIMULATOR TESTS

4.1 Test Set-Up

As noted in Sec. 3, the test structure used was a five-story model building (refer back to Fig. 3.1). The model building is 224.0" in height and 52.0" on each side. Diagonal braces with SMA dampers were bolted to the gusset plates welded to the girders (Fig. 4.1). The acceleration and absolute displacement in the horizontal direction were measured on the east and west sides of the concrete base and on each floor of the building. In addition, the displacement δ, across the damper between the second and third floors on both sides of the building, was also measured. The placement of the displacement and acceleration measurement devices is shown in Fig. 4.2. Temposonic displacement transducer's and Endevco accelerometer's were used for the displacement and acceleration measurements. Strain was also measured using strain gauges on the top and bottom of the girders of the second and third floors, where the strain was expected to be the largest.

A banded white noise test was run to determine the frequency response function of the structure. This frequency response function was then used to construct simulated ground motions of the Hachinohe, Olympia, El Centro and Quebec earthquake records. To prevent damage to the structure, each ground motion was initially run with a conservatively small peak acceleration of 0.06g's. The magnitudes of the ground motions were then increased until it was determined that the structure would be damaged by any further

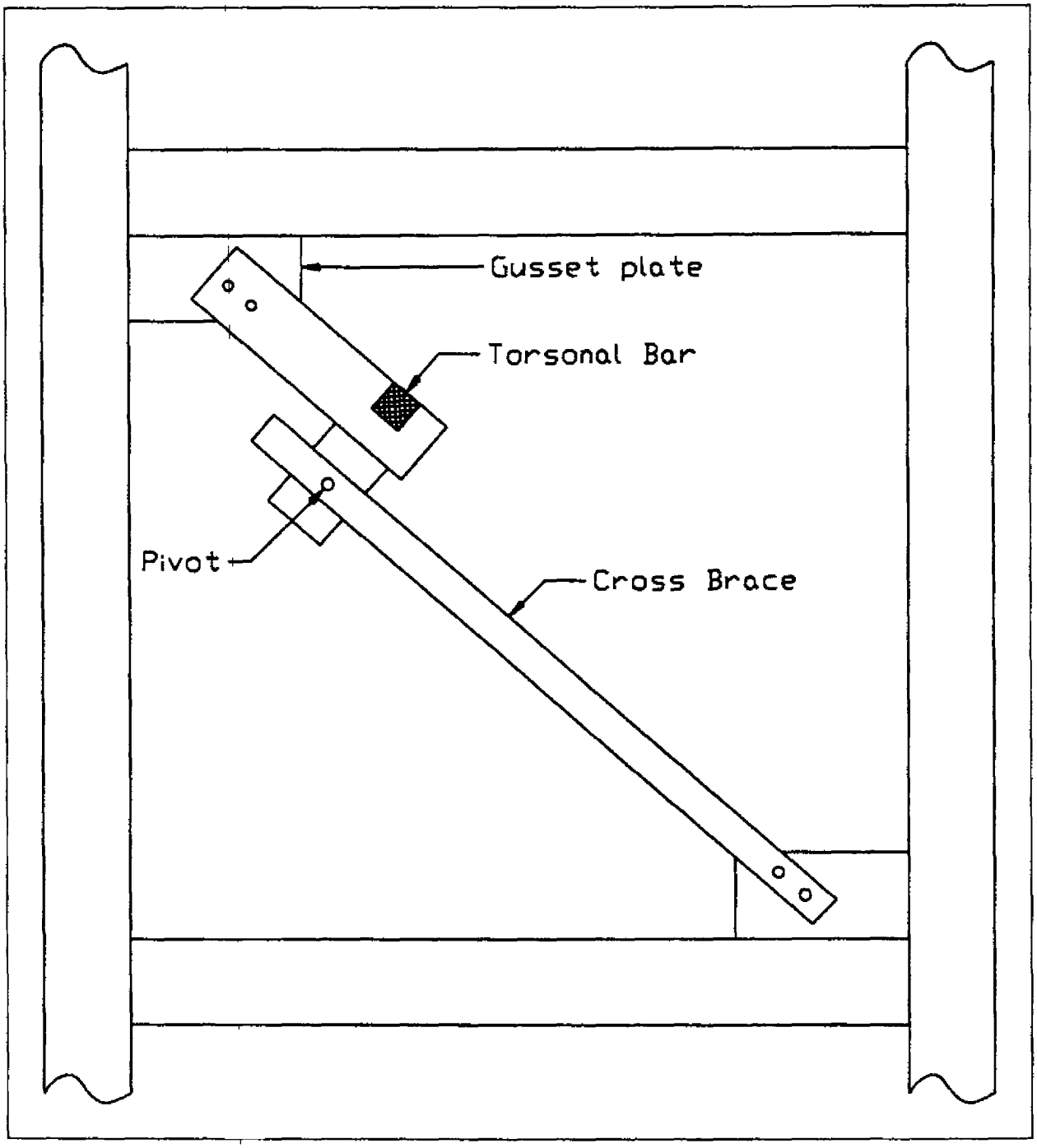

Fig. 4-1 Placement of SMA Dampers Between Floors

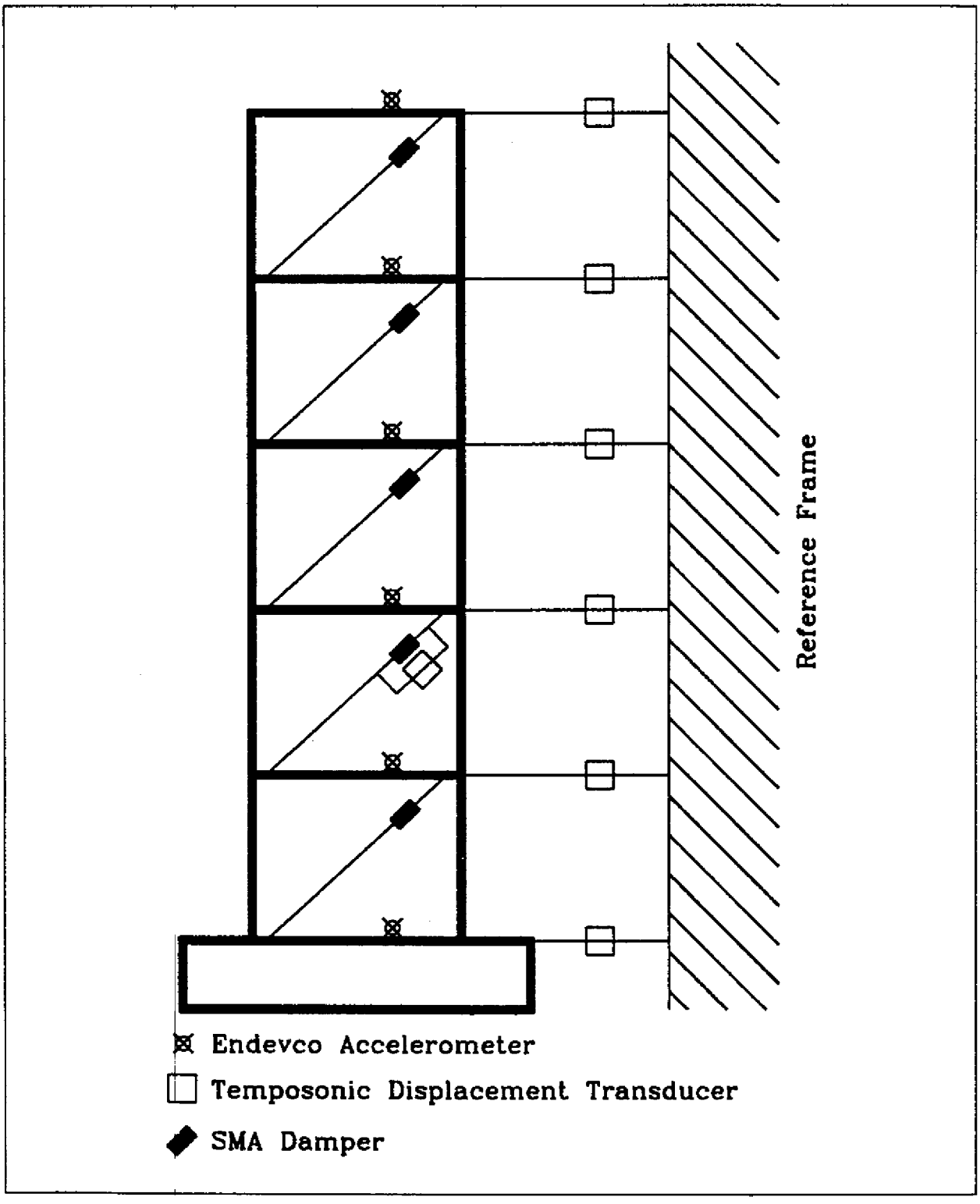

Fig. 4-2 Instrumentation of Model Structure

increase. The maximum inter-story drift and maximum strain measured during the tests determined whether or not an earthquake of greater magnitude would be run. All four earthquakes and banded white noise were run with peak accelerations of 0.06g, 0.12g, 0.24g and 0.36g. In addition, the structure was subjected to banded white noise and the four ground motions at 0.06g's with no dampers.

4.2 Test Results

Bar graphs, which compare the damped to undamped building responses for the four earthquake records, are given in Figs. 4.3-4.15. Figs. 4.3-4.6 present the maximum relative floor displacements, with and without dampers, for the four earthquake records. Figs 4.7-4.10 present the maximum floor accelerations for the same cases. Finally, Figs. 4.11-4.15 present the maximum inter-story drift for these same cases. Table 4.1 summarizes the results of Figs. 4.3-4.15 by listing the maximum responses of the undamped structure and the percent reduction of responses of the damped structure, for all the above mentioned cases.

In Sec. 3.3, we noted that larger damper displacements resulted in larger energy absorbing hysteresis loops. It was also noted that the damper stiffness decreases with increasing deflections. This change in stiffness and energy absorbing hysteresis loops with deflection, was expected to cause a change in the natural frequency and damping ratio of the building as the magnitudes of the ground motions increased. Since the damper stiffness decreases with larger deformation (Sec. 3.3), the natural

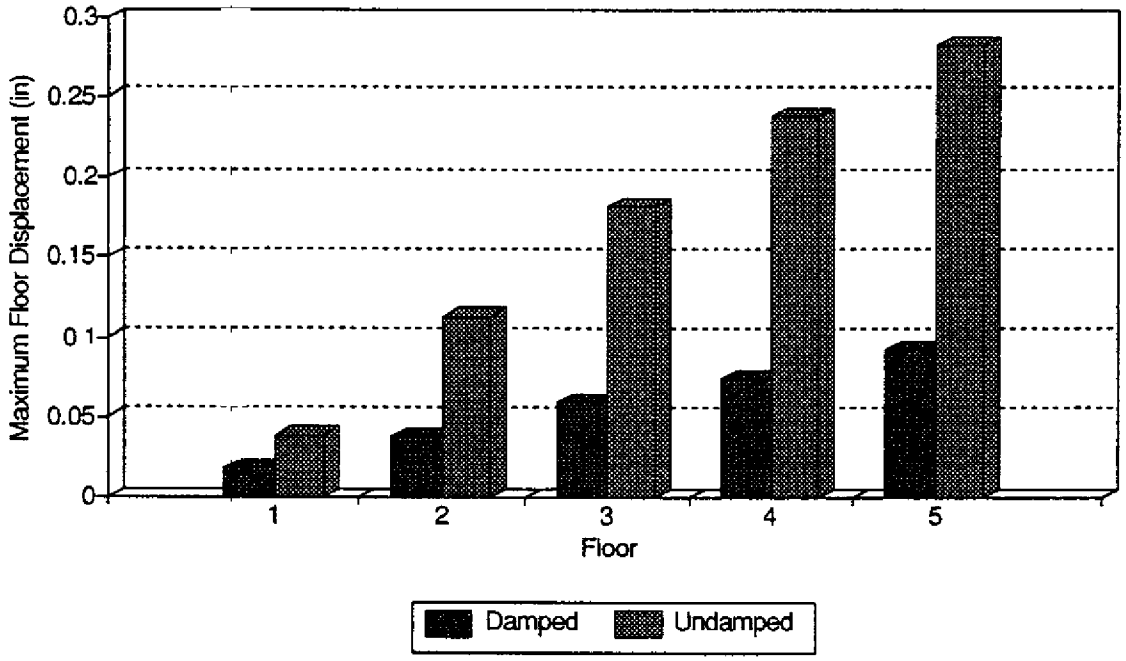

Fig 4-3 Max Floor Disp. (0.06 El Centro)

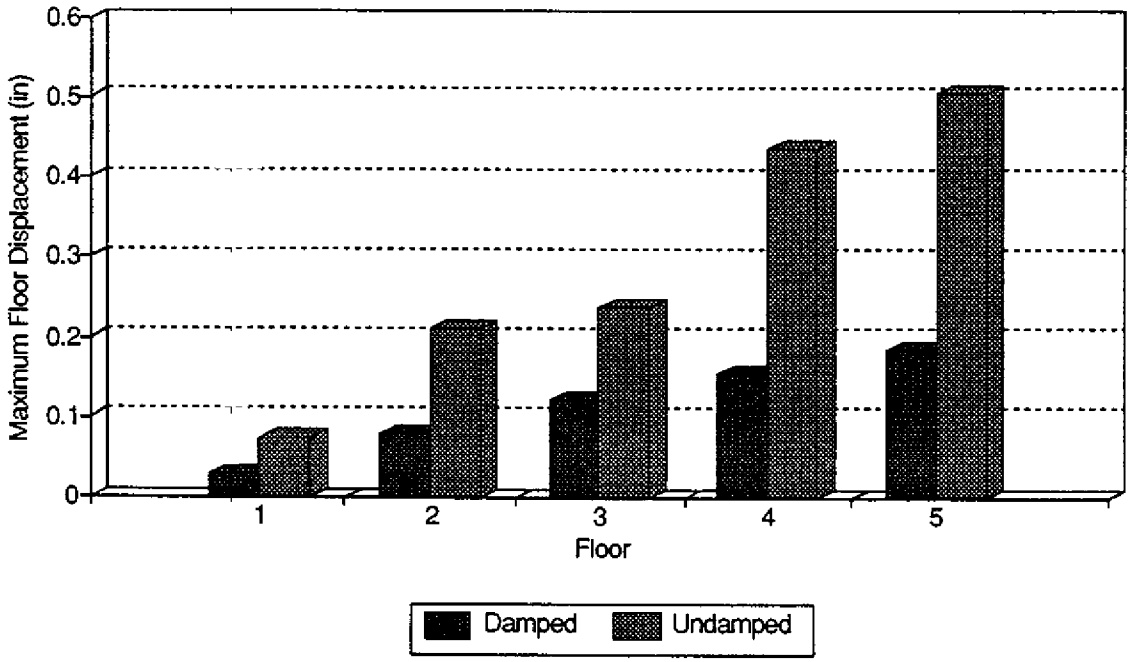

Fig 4-4 Max Floor Disp. (0.06 Hachinohe)

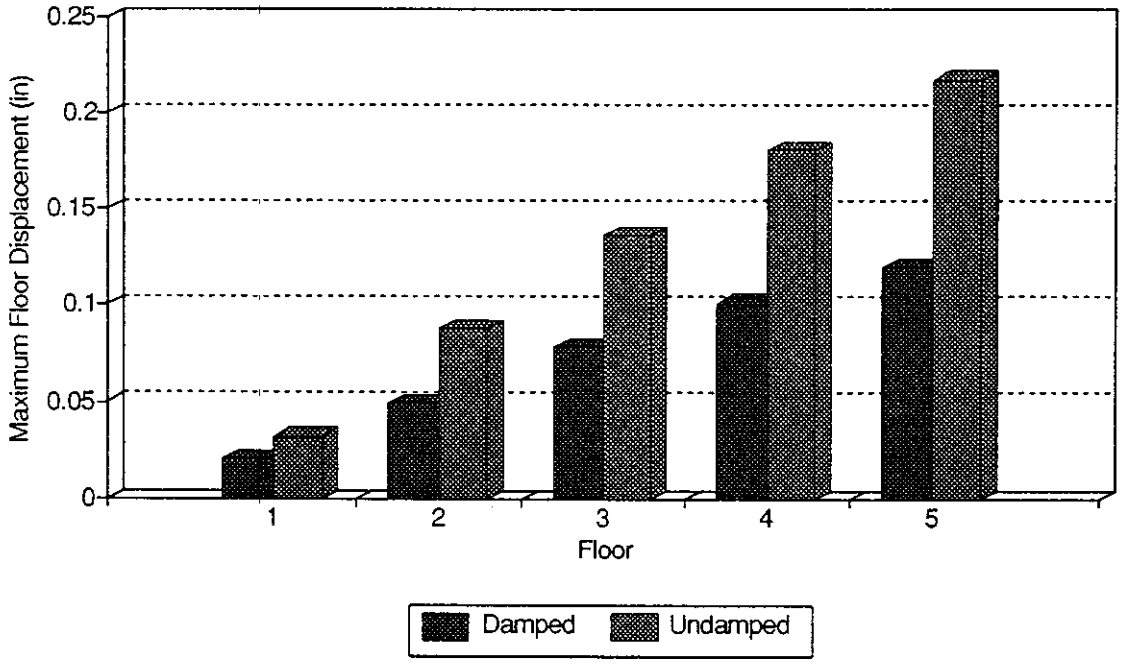

Fig 4-5 Max Floor Disp. (0.06 Olypia)

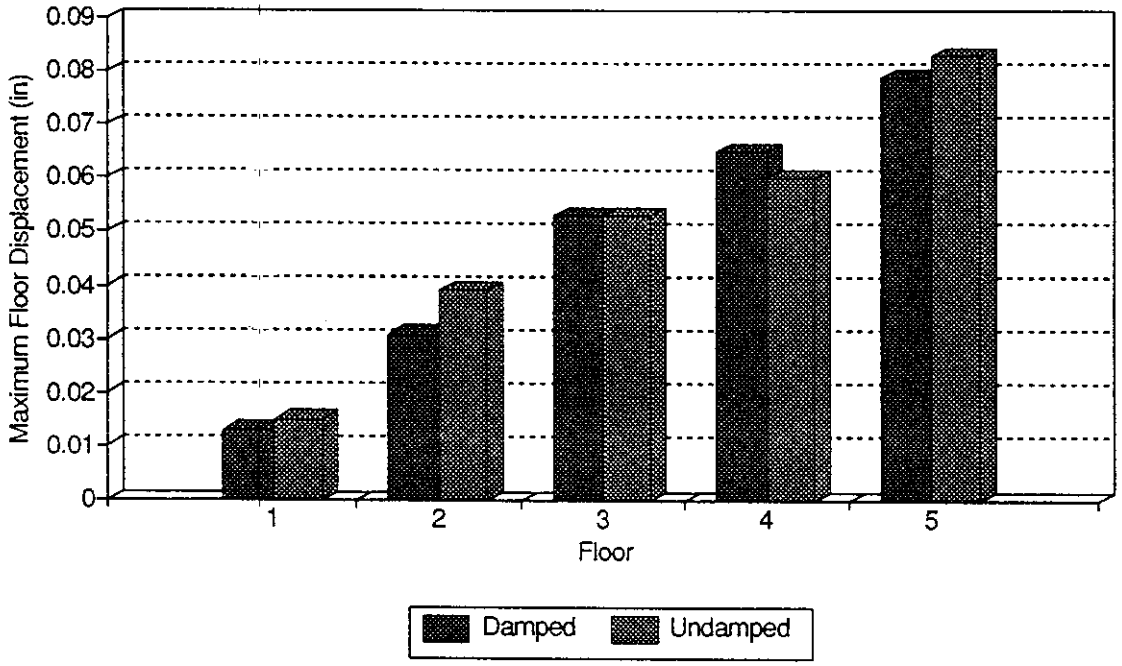

Fig 4-6 Max Floor Disp. (0.06 Quebec)

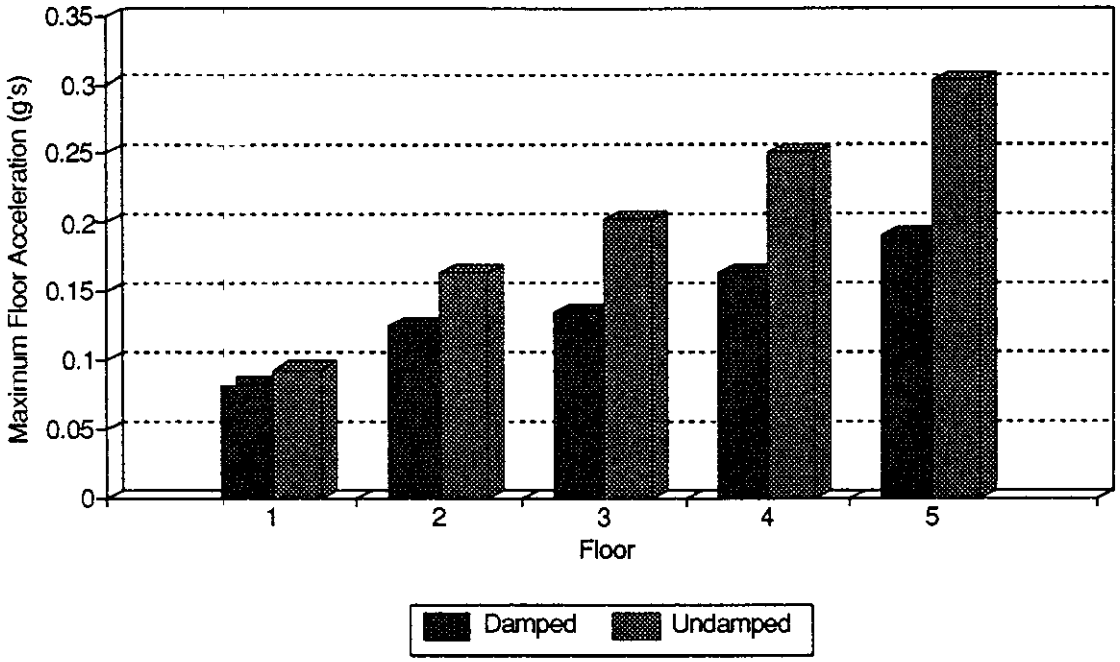

Fig 4-7 Max Floor Acceleration (0.06 El Centro)

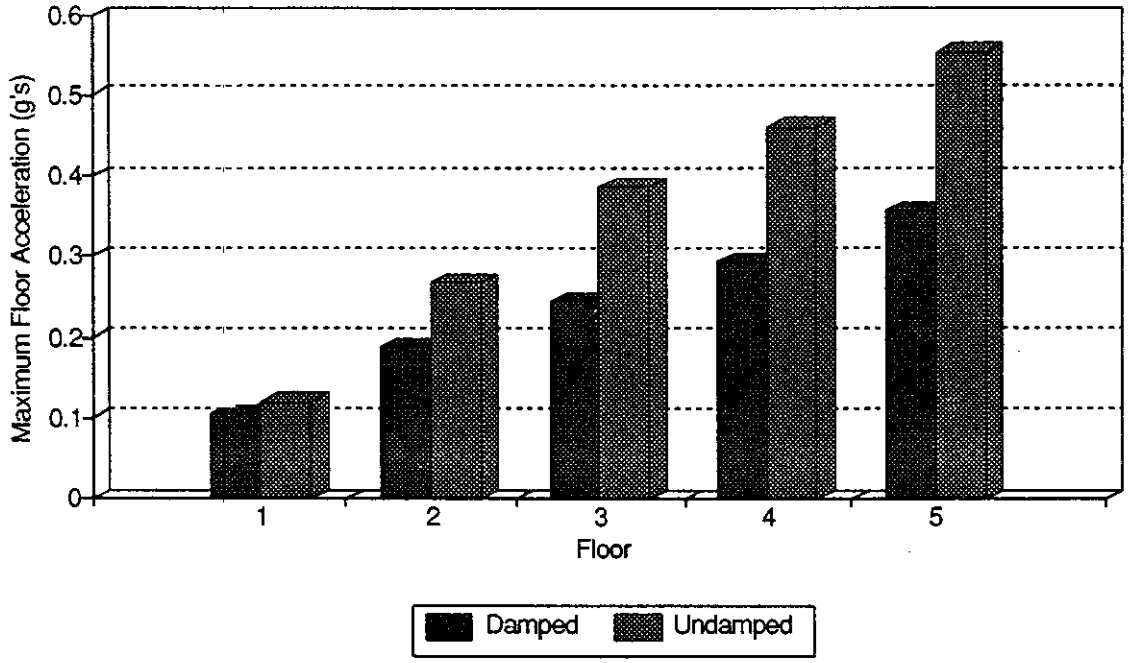

Fig 4-8 Max Floor Acceleration (0.06 Hachinohe)

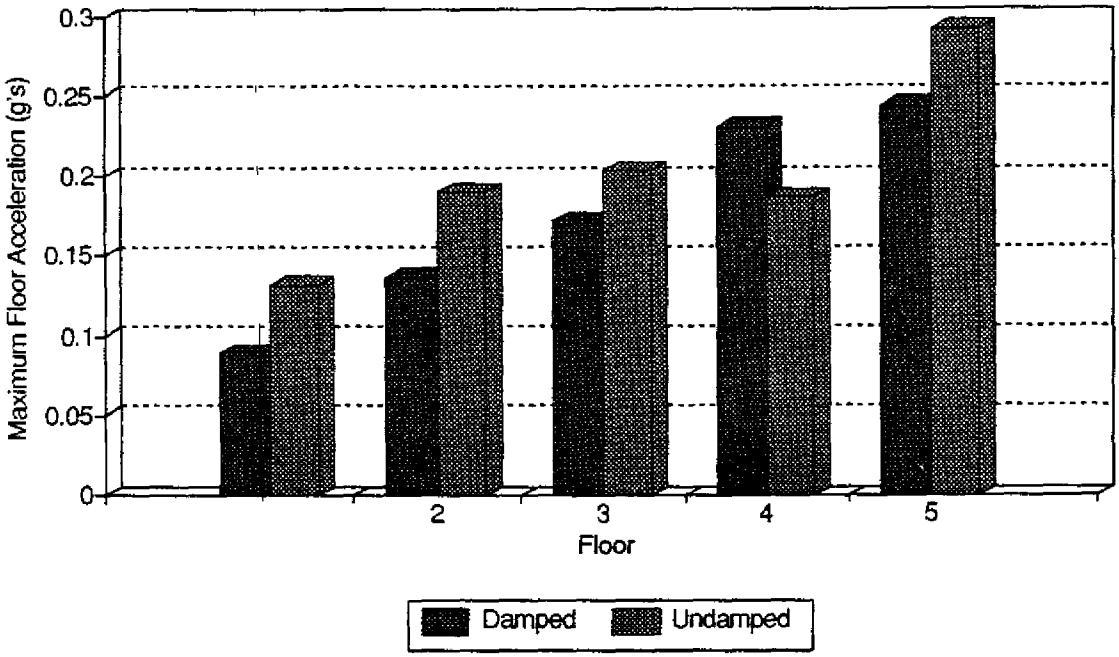

Fig 4-9 Max Floor Acceleration (0.06 Olypia)

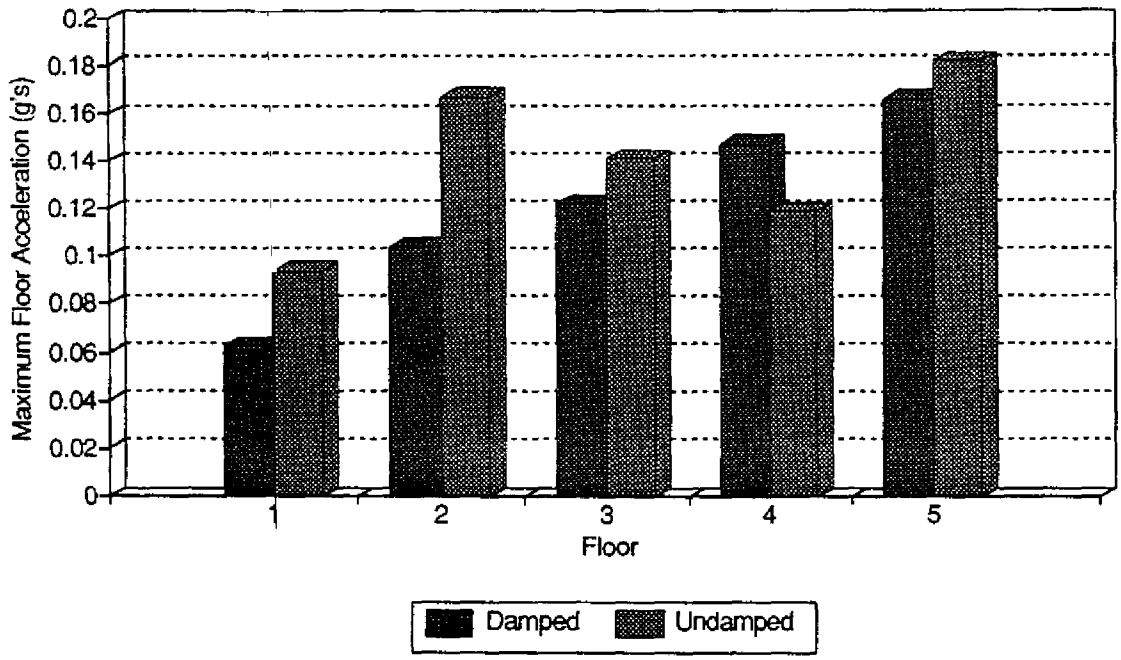

Fig 4-10 Max Floor Acceleration (0.06 Quebec)

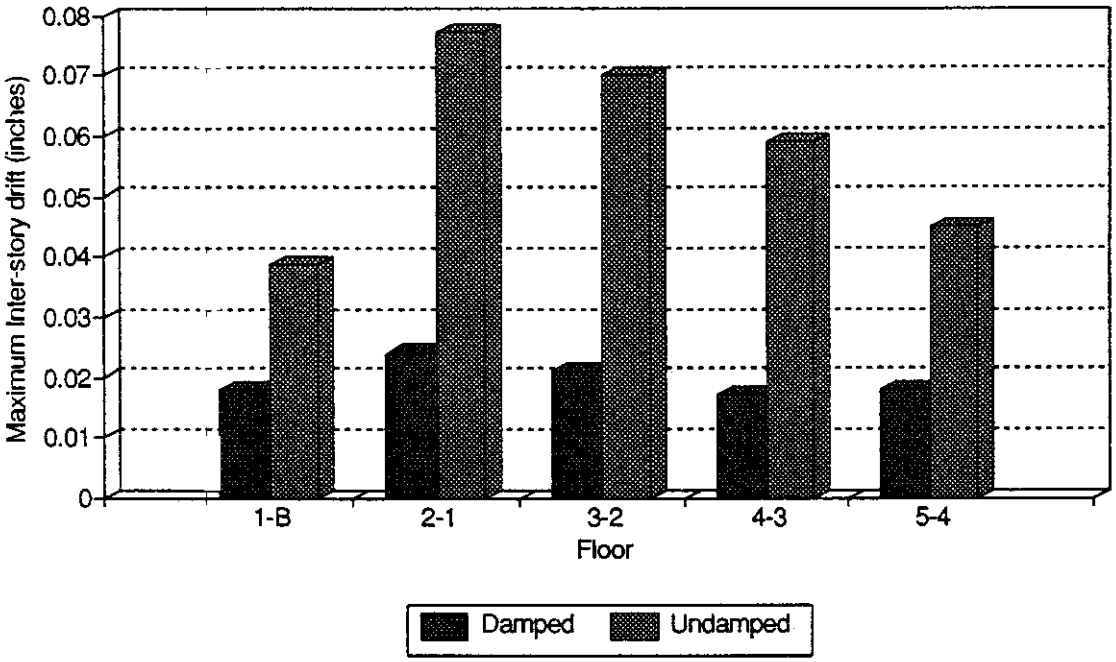

Fig 4-11 Max Inter-Story Drift (0.06 El Centro)

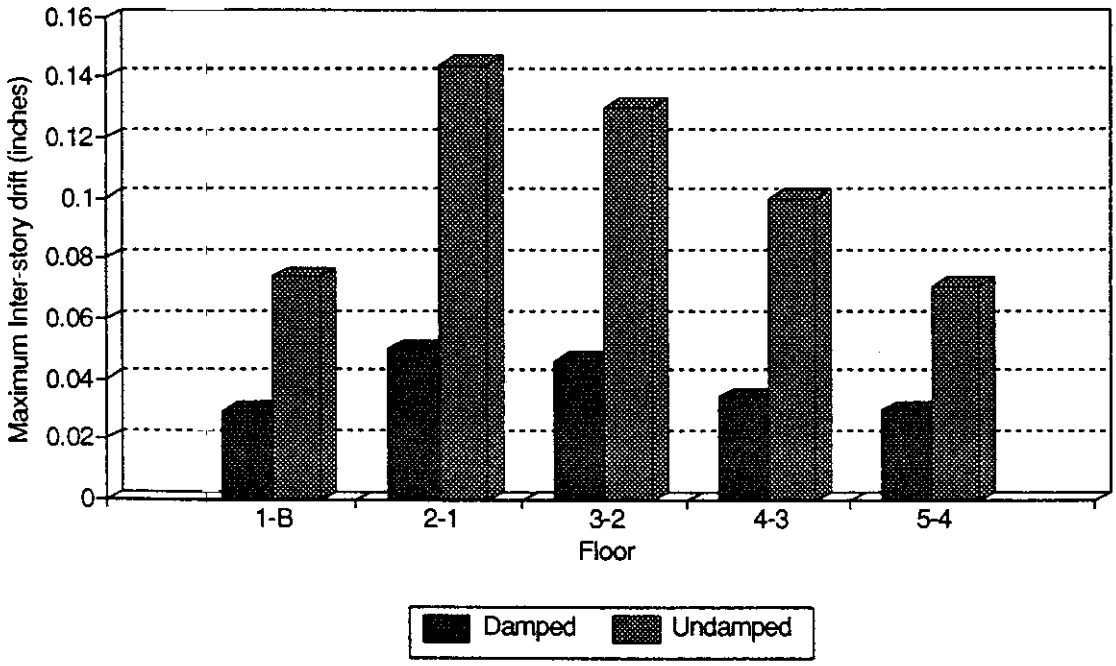

Fig 4-12 Max Inter-Story Drift (0.06 Hachinohe)

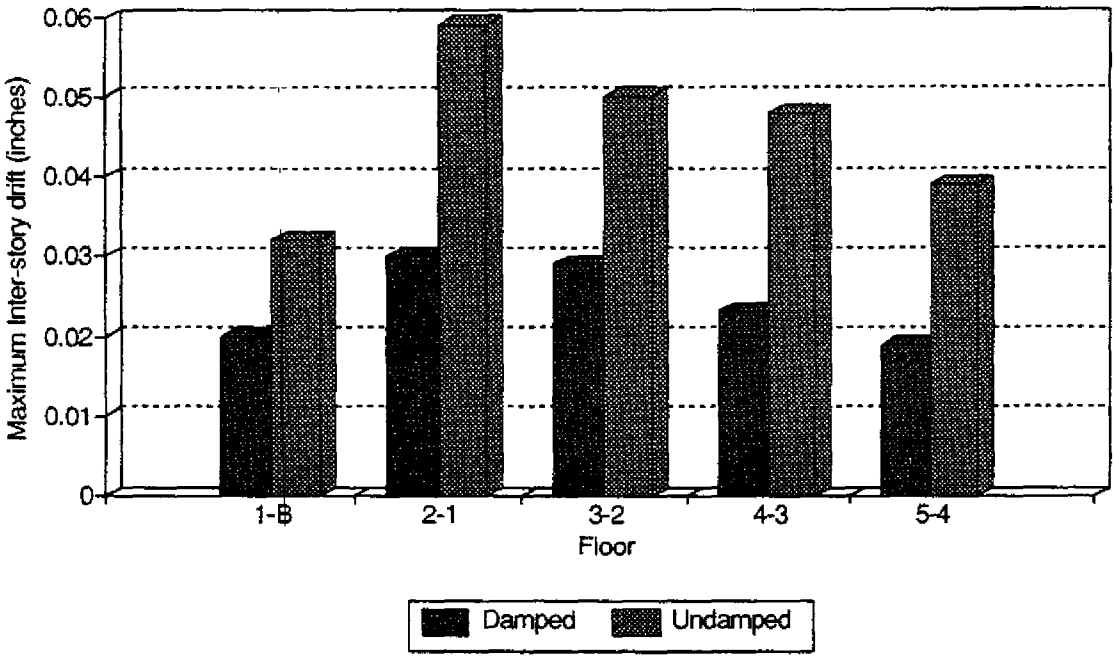

Fig 4-13 Max Inter-Story Drift (0.06 Olypia)

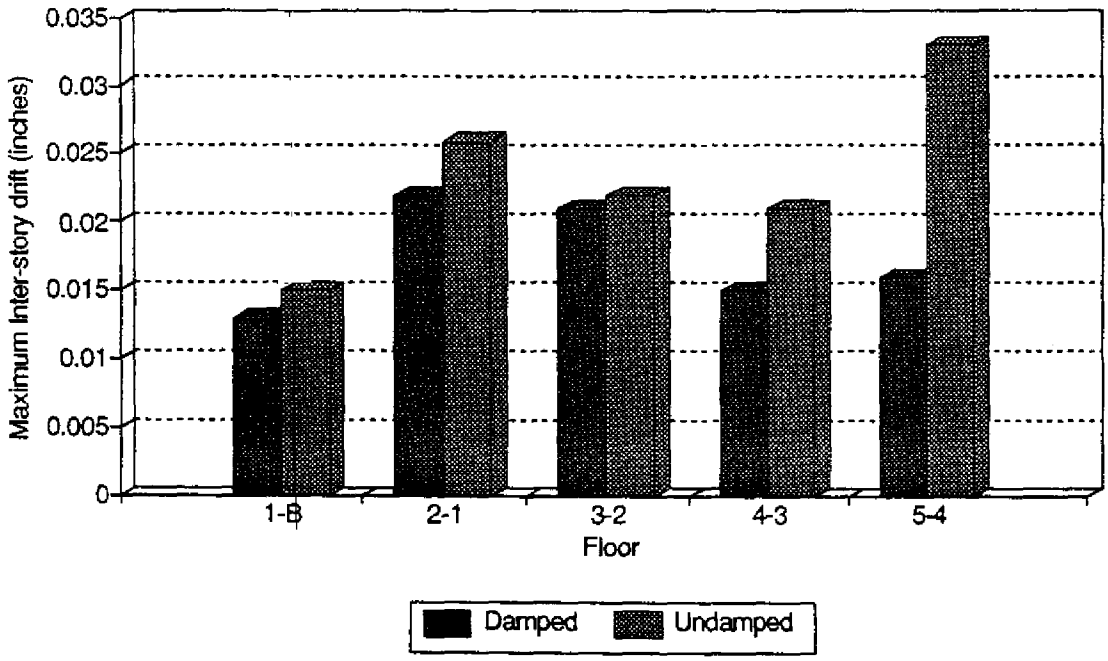

Fig 4-14 Max Inter-Story Drift (0.06 Quebec)

Maximum Response	Floor Level	Earthquake's with 0.06g max acceleration			
		Hachinohe		El Centro	
		Undamped	% Reduction	Undamped	% Reduction
Relative Floor Disp. (inch)	1	0.074	60.4%	0.039	53.4%
	2	0.211	62.7%	0.113	66.4%
	3	0.237	48.9%	0.182	67.6%
	4	0.436	64.4%	0.238	68.9%
	5	0.507	63.5%	0.283	67.5%
Maximum Floor Acc. (g's)	1	0.119	12.6%	0.093	11.8%
	2	0.267	29.2%	0.163	23.3%
	3	0.387	36.7%	0.203	33.5%
	4	0.461	36.2%	0.251	34.7%
	5	0.554	35.6%	0.303	37.3%
Inter-Story Drift (inch)	1-B	0.074	60.4%	0.039	53.4%
	2-1	0.144	65.3%	0.077	68.8%
	3-2	0.130	64.6%	0.070	70.0%
	4-3	0.100	66.0%	0.059	71.2%
	5-4	0.071	57.7%	0.045	60.0%
		Quebec		Olympia	
		Undamped	% Reduction	Undamped	% Reduction
Relative Floor Disp. (inch)	1	0.015	13.3%	0.032	37.5%
	2	0.039	20 5%	0.088	44.3%
	3	0.053	0.0%	0.136	42.6%
	4	0.060	-8.3%	0.181	44.2%
	5	0.083	4.8%	0.217	44.7%
Maximum Floor Acc. (g's)	1	0.094	33.0%	0.131	32.1%
	2	0.167	37.7%	0.190	28.4%
	3	0.141	13.5%	0.203	15.3%
	4	0.119	-23.5%	0.187	-23.5%
	5	0.182	8.8%	0.292	16.4%
Inter-Story Drift (inch)	B-1	0.015	13.3%	0.032	37.5%
	2-1	0.026	15.4%	0.059	49.2%
	3-2	0.022	4.5%	0.050	42.0%
	4-3	0.021	28.6%	0.048	52.1%
	5-4	0.033	51.5%	0.039	51.3%

Table 4-I Summary of Dynamic Response of Model Building

frequency of the building was also expected to decrease under the larger earthquakes. Fig. 4.15a shows the expected decrease in the natural frequency with increase of the base excitation. Under larger deformation, larger energy absorbing force deflection cycles are experienced which causes an increase in the damping ratio. Fig. 4.15b shows such an increase in damping with larger earthquakes.

It should be noted that the above mentioned damping ratios were calculated by the half-power method [5] for the first mode of vibration only Since the damping ratio is less the 15%, the half-power method can be considered accurate. A plot of a typical third floor acceleration frequency transfer function with SMA dampers (Fig. 4.16), reveals the first and second modes of vibration clearly. However, the frequency response of the second mode of vibration is less then half that of the first mode. Therefore, the discussion of results will be limited to the first mode of vibration, since it dominates the dynamic response of the structure. In addition to the damped third floor transfer function the undamped the bare frame transfer function the undamped third floor acceleration frequency transfer function (Fig. 4.17) is shown for comparison. The bare frame transfer function is characterized by a tall and narrow spike at 3.2 Hz. This indicates little damping. The frequency response of the SMA damped building is wider and shorter which shows an increased damping from the undamped case.

Fig. 4-15a
Natural Frequency vs Base Excitation

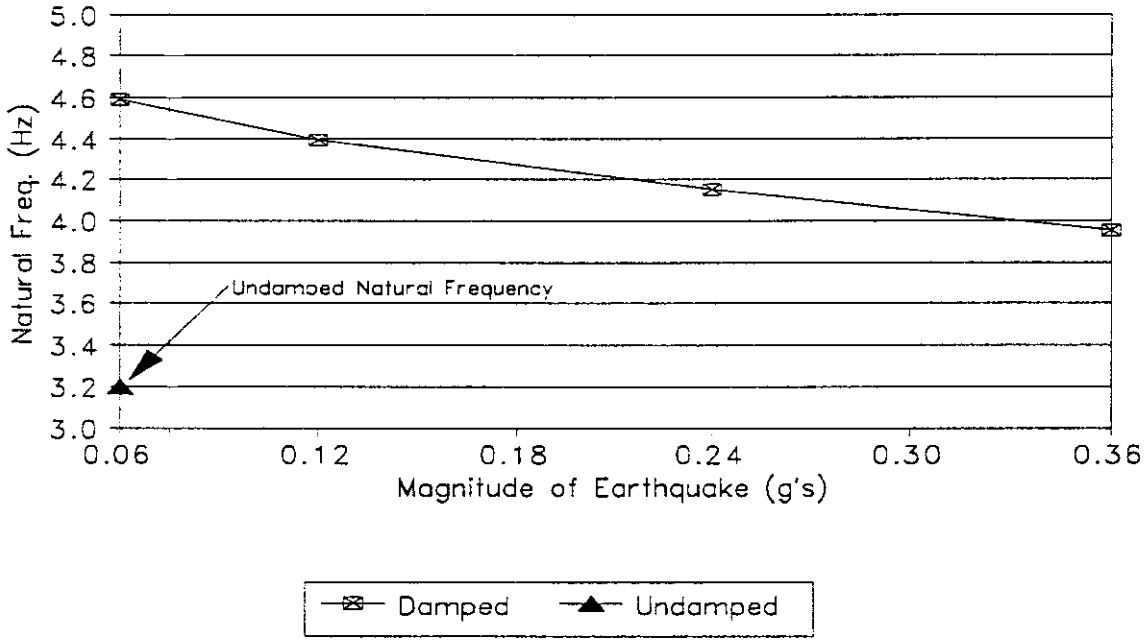

Fig. 4-15b
Damping Ratio vs Base Excitation

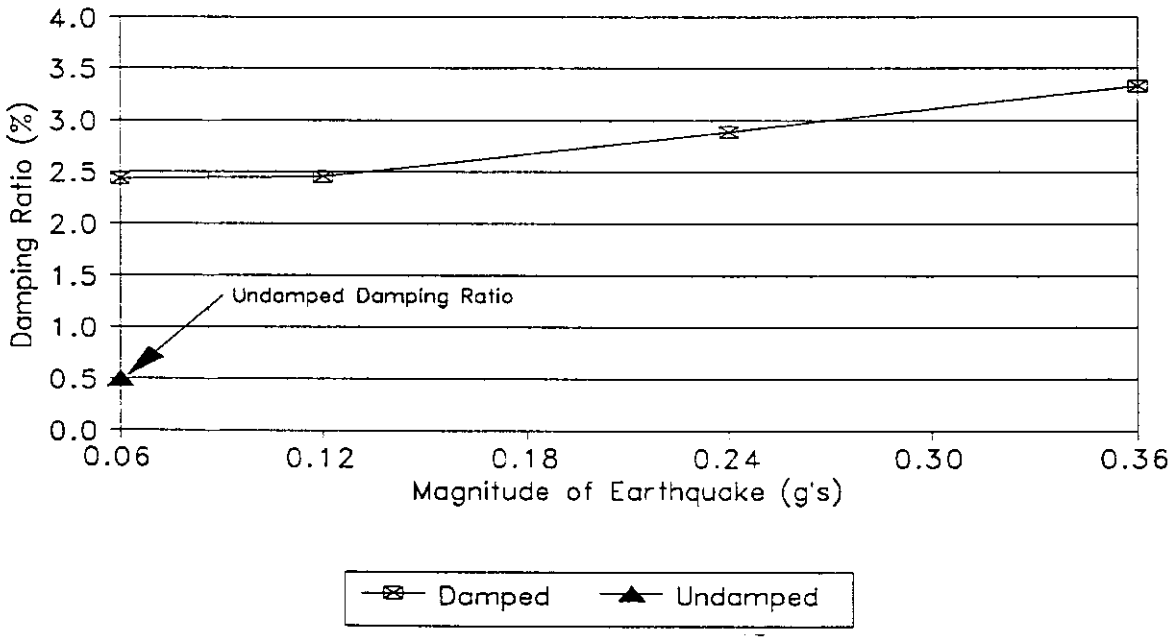

Fig 4-15 Natural Frequency and Damping Ratio

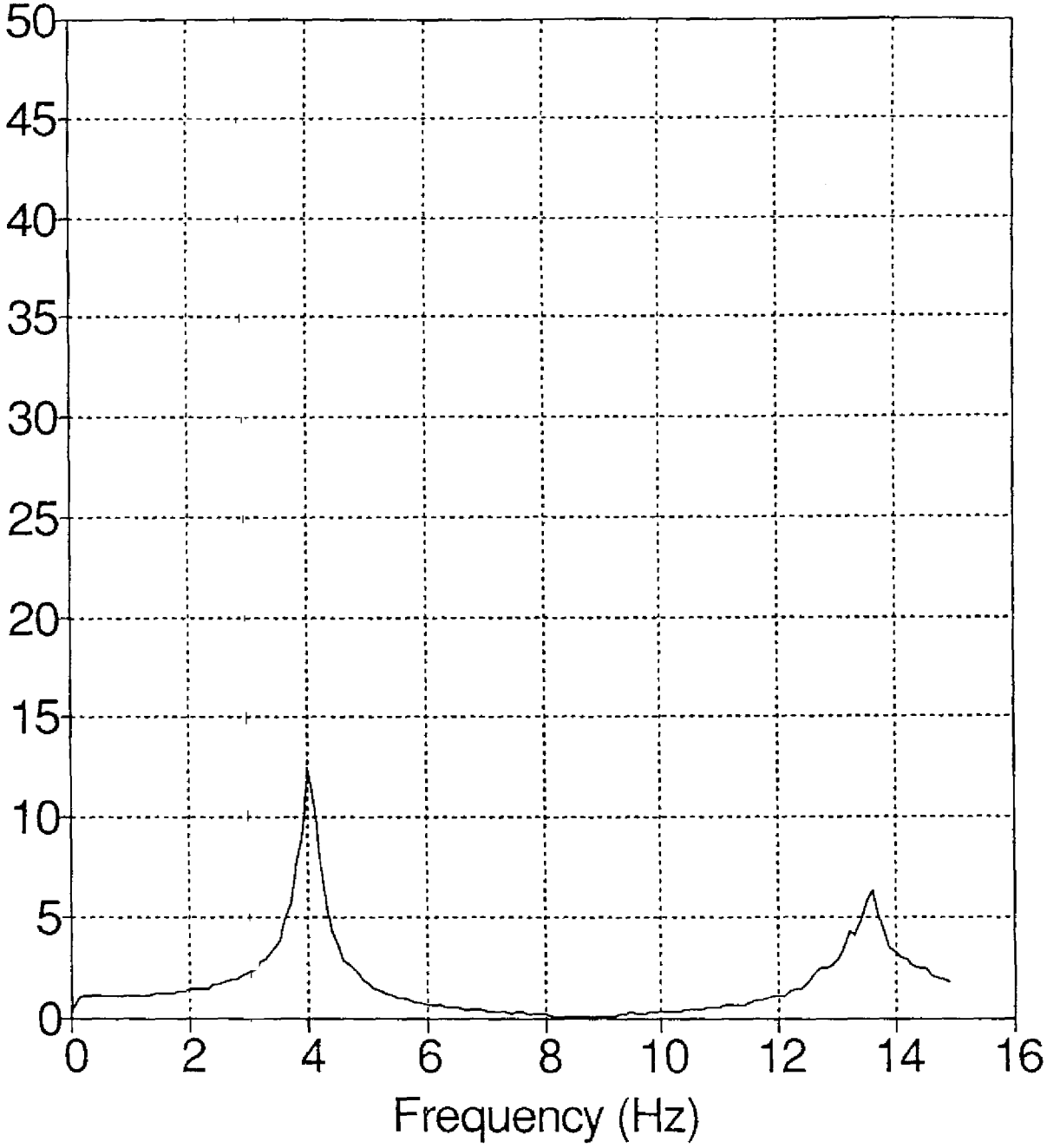

Fig 4-16 Frequency Response of Damped Building

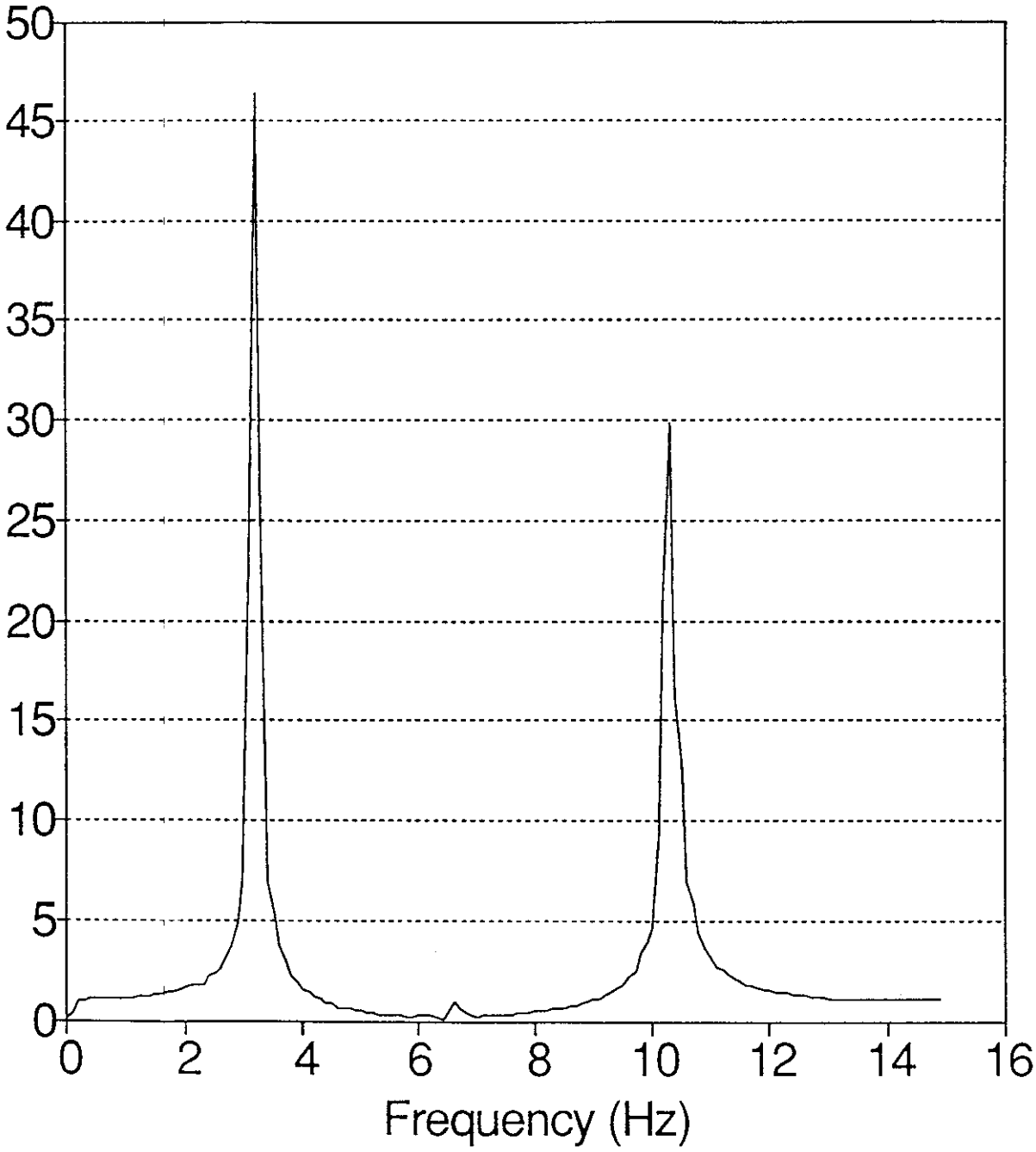

Fig 4-17 Frequency Response of Undamped Building

4.3 Discussion of Results

It seems apparent from an examination of Table 4.1 that the effectiveness of the damper varies with the earthquake. For instance, the percent reduction of the maximum relative floor displacement due to the Hachinohe ground motion averaged over the five floors is 60.0%, while same averaged percent reduction for the Quebec earthquake case is only 6.1%. In fact, the forth floor maximum relative floor displacement and maximum acceleration of the damped building was greater then the response of the undamped building in the Quebec earthquake case. The other floors maximum responses as well as the inter-story drift response for all floors, however, were smaller in the damped case then the undamped case. These sizable differences can be accounted for by noting that the frequency contents of the four ground motions are different. The Quebec earthquake has a larger content of higher frequencies then the Hachinohe earthquake. Since the SMA dampers increase the natural frequencies of the building (Fig. 4.15a), the SMA dampers will be more effective against earthquakes with lower frequencies.

The calculated damping ratios are less dependent upon the frequency content of the earthquake record. Fig. 4.15b shows an increase of damping over the undamped case. However, the damping for SMA dampers is not as great as for viscoelastic dampers. Viscoelastic dampers have been shown [5] to yield a damping ratio between 5% and 14%, depending on the temperature of the viscoelastic material, for the same five story model building. Whereas the SMA damper properties are not highly temperature

dependent, the damping measured was less than for the viscoelastic dampers at their least favorable temperature. Since the SMA damper was designed to maximize the benefits of the Shape Memory Material properties of Cu-Zn-Al (Sec. 3.3), there is no evidence to indicate that a redesign of the damper would result in improved damping.

In spite of the above drawbacks, the potential for effective SMA damping is apparent. The dampers did mitigate the building's motion and the building was safely tested with the SMA dampers at levels where the building would have been severely damaged without the dampers In addition, the test results indicate that the SMA damper is probably best suited for base isolation applications. One of the features of the SMA damper is the self centering hysteresis loop. It became evident that this feature is not effectively utilized in structural damping, because the building's inherent stiffness creates a self centering force that is much greater than the damper's. However, in base isolation this self centering property would be of great benefit, since the base isolation device acting alone must restore the building to its original position.

Another indication that the SMA damper would be useful in base isolation is the change in natural frequency of the building with increased levels of base excitation (Fig. 4.15a). A base isolation device should be stiff for small deflection, so that wind loading and small tremors will not cause the building to move excessively. In the event of a large earthquake, the stiffness should reduce and allow the building greater mobility to isolate itself from the

ground motion. The decrease in natural frequency of the damped building (Fig. 4.15a) with increased base excitation indicates a corresponding decrease of damper stiffness with increased damper deflection. This same change in damper stiffness was also noted in Sec. 3.3.

SECTION 5

SUMMARY AND CONCLUSION

The results of experimental studies on the material properties of the shape memory material (SMA) Cu-Zn-Al have been presented and analyzed. Experimental results on the seismic behavior of a Cu-Zn-Al SMA damped steel-frame 2/5 scale model structure have also been presented. In addition, a discussion of the advantages of the torsion bar SMA damper over other SMA damper designs was included.

The material test results show that this composition of Cu-Zn-Al has a superelastic stress strain relation for a very limited number of cycles. After a few cycles, the internal friction will increase and cause a hysteretic material behavior with a very small amount of spring back. The final hysteretic stress strain behavior was found to be caused by martensitic transformation rather than by slip/glide dislocation motion.

The seismic test results demonstrated that Cu-Zn-Al dampers are effective at mitigating the 2/5 model five story building's response to various ground motions. The results were compared to results of tests done with viscoelastic dampers, and it was concluded that the Cu-Zn-Al dampers were not as effective as the viscoelastic dampers. The test results of the structural dampers indicated that the SMA dampers are better suited for base isolation.

SECTION 6
REFERENCES

1. Roark, Raymond J., and Young, Warren C., "Formulas for Stress and Strain fifth edition," McGraw-Hill Inc., 1975.

2. Shigley, Joseph E., and Mitchell, Larry D., "Mechanical Engineering Design-Fifth Edition," McGraw-Hill Inc., 1983.

3. Ugural, A. C., and Fenster, S. K., "Advanced Strength and Applied Elasticity-Second SI Edition," Elsevier, 1987.

4. Shames, Irving H., "Introduction to Solid Mechanics," Prentice-Hall Inc., 1974.

5. Chang, K.C., Soong, T.T., Oh, S-T., and Lai, M.L., "Seismic Response of a 2/5 Scale Steel Structure with Added Viscoelastic Dampers," Technical Report NCEER-91-0012, 1991.

5. Clough, Ray W., and Penzien, Joseph, "Dynamics of Structures," McGraw-Hill Inc., 1975.

6. Graesser, Edward J., "Multi-Dimensional Modeling of Hysteretic Materials Including Shape Memory Alloys: Theory and Experiment," Ph.D. Dissertation, SUNY Buffalo, Buffalo, NY, January, 1990.

7. Duerig, T. W., Melton, K. N., Stöckel, D., Mayman, C. M., "Engineering Aspects of Shape Memory Alloys," Butterworth-Heinemann Ltd., 1990.

8. Filiatrault, A., Cherry, S., "Comparative Performance of Friction Damped Systems and Base Isolation Systems for Earthquake Retrofit and Aseismic Design," Earthquake Engineering and structural Dynamics, 1988, Vol. 16, pp. 389-416.

9. Zhang, Ri-Hui., Soong, T.T. Mahmood, P., "Seismic Response of steel Frame Structures with Added Viscoelastic Dampers," Earthquake Engineering and structural Dynamics, 1989, Vol 18, pp. 389-396.

10. Roik, K., Dorka, U., Dechent, P., "Vibration Control of Structures Under Earthquake Loading By Three-Stage Friction-Grip Elements," Earthquake Engineering and structural Dynamics, 1988, Vol. 16, pp. 501-521.

11 Malushte, S.R., Singh, M.P., "A Study Of Seismic Response Characteristics Of Structures With Friction Damping," Earthquake Engineering and structural Dynamics, Vol. 18, pp. 767-783.

12 Hna, Ycn S., Kim, Young G., "The Effects of Boron and Aging on Mechanical Properties and Martensitic Temperatures in Cu-Zn-Al Shape-Memory Alloys," Scripta Metallurgica, 1987, Vol. 21, pp 947-952.

13 Graesser, E. J., Cozzarelli, F. A., "A multidimensional Hysteretic Model for Plastically Deforming Metals in Energy Absorbing Devices," Technical Report NCEER-91-0006, 1991.

14 Fletcher, A. J., Thomas, D. L., "Solid-State Transformations in Certain Copper-Aluminum-Zinc Alloys." Journal of the Institute of Metals, 1970, Vol 98, pp 188-192.

15 Itoh, I., Hikage, T., "Dezincification Mechanism of Brass in Vacuum at High Temperature," Transactions of the Japan Institute of Metals, 1976, Vol. 17, pp 165-169.

16 Graesser, E. J., Cozzarelli, F. A., "Shape Memory Alloys as New Materials for Aseismic Isolation," Journal of Engineering Mechanics Vol. 117, No. 11, pp 2590-2688, Nov., 1991.

17 Kajiwara, S., Kikuchi, T., "Dislocation Structures Produced by Reverse Martensitic Transformation in a Cu-Zn Alloy," Acta Metall., 1982, Vol. 30, pp 589-598.

APPENDIX A

DAMPER ASSEMBLY

All parts of the damper are made from steel, except the torsion bar which is made from Cu-Zn-Al SMA (Fig. A-1). After the Cu-Zn-Al has been machined into the torsion bar, whose dimensions are given in Fig. A-1, it is heat treated by the heat treatment given in Sec. 2. After the heat treatment, the Cu-Zn-Al bar must be hand sanded to remove the damaged surface.

Assembly

1. Slide the center square section of the torsion bar (Fig. A-1) in the grove of the torsion arm (Fig. A-2)
2. Take the large clamp (Fig. A-5) and align its holes with the tapped screw holes of the torsion arm. Screw the large clamp in tightly. This should prevent the torsion bar from sliding out of the grove in the torsion arm.
3. Place a small amount of oil on the pin (Fig. A-5), and then slide the pin through the reamed hole in the torsion arm.
4. Slide a connector (Fig. A-3) over the pin to each side of the torsion arm.
5. Next fit the torsion arm into the groves of the holder (Fig. A-4).
6. Screw the small clamps to the holder to clamp the torsion bar in place.
7. Bolt with 1/4 inch bolts the holes labeled A in brace A (Fig.

A-6) to the holes labeled A in the holder. Bolt with 1/4 inch bolts the holes labeled B (Fig. A-7) in brace B to the holes labeled B in the holder.

8. Arrange brace D and brace E so that the two holes near the center of the bar are aligned. Place a spacer between the bars and bolt brace D to brace E with a spacer in between.

9. Place a double spacer between brace D and brace E aligned with the 1.25" space holes. Align the connectors with the 1.25" spaced holes of brace D and Brace E and bolt in place. Note that these bolts should pass through these components in the following order: connector, brace, double spacer, brace, connector.

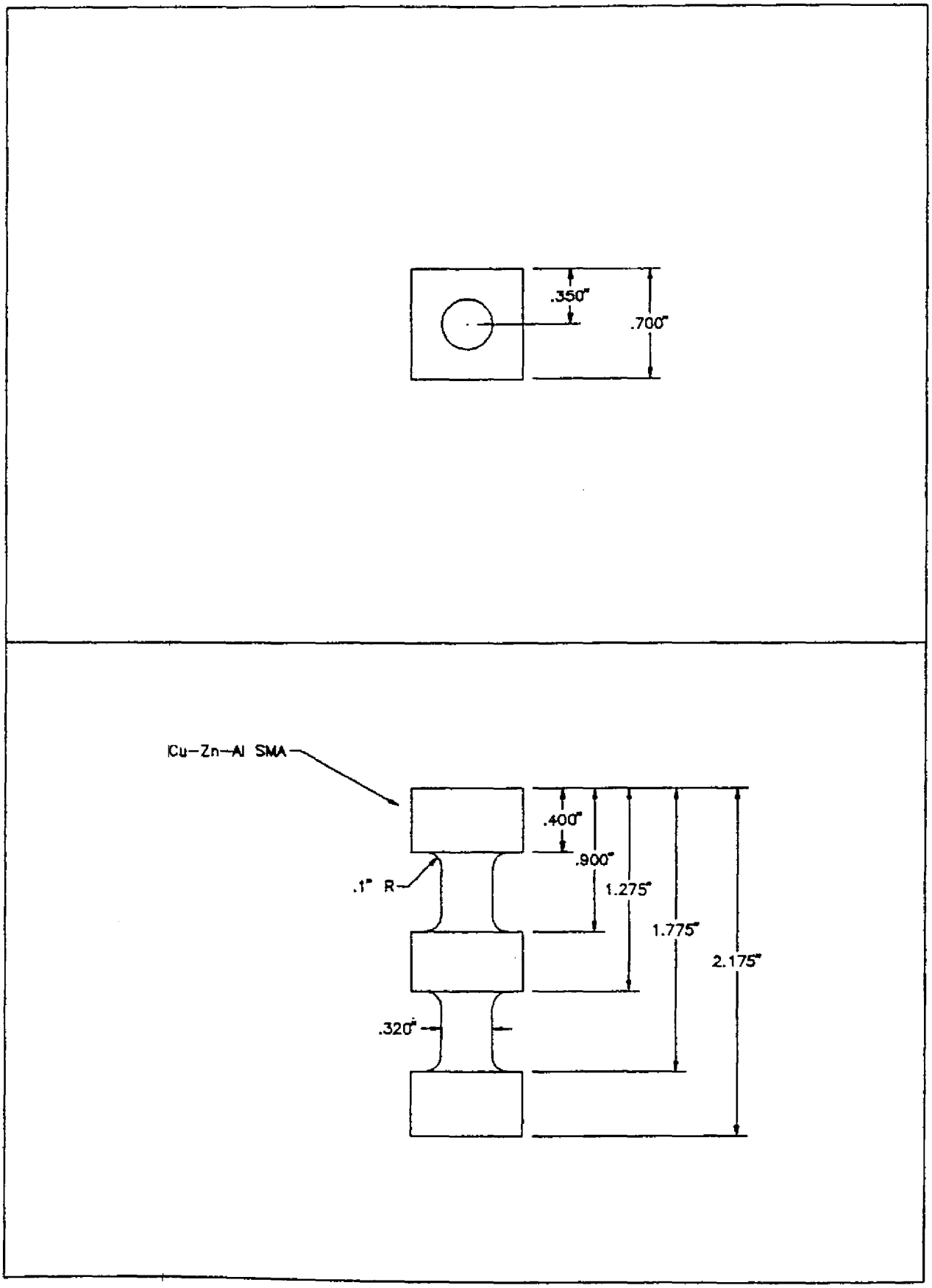

Fig. A-1 Torsion Bar

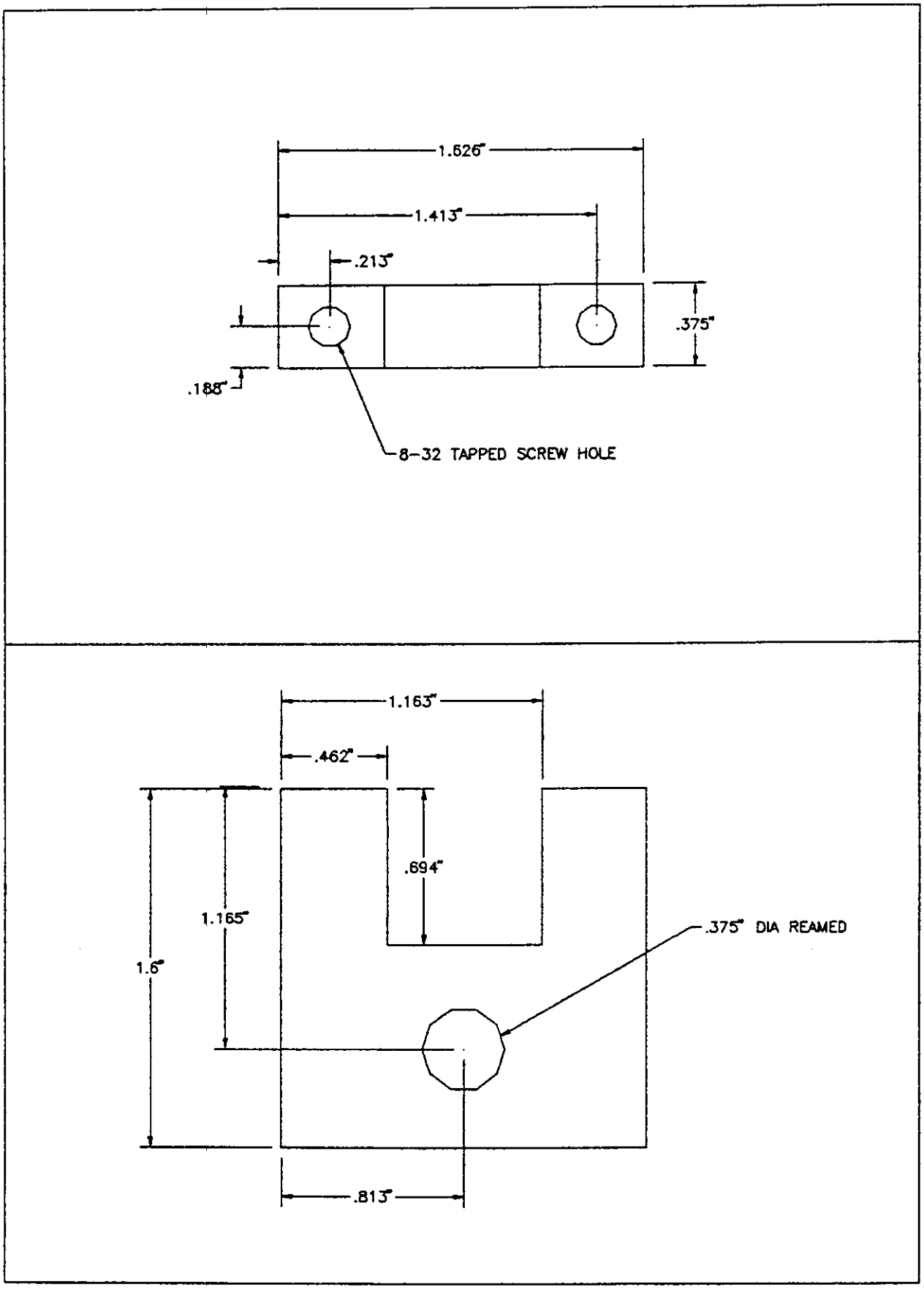

Fig. A-2 Torsion Arm

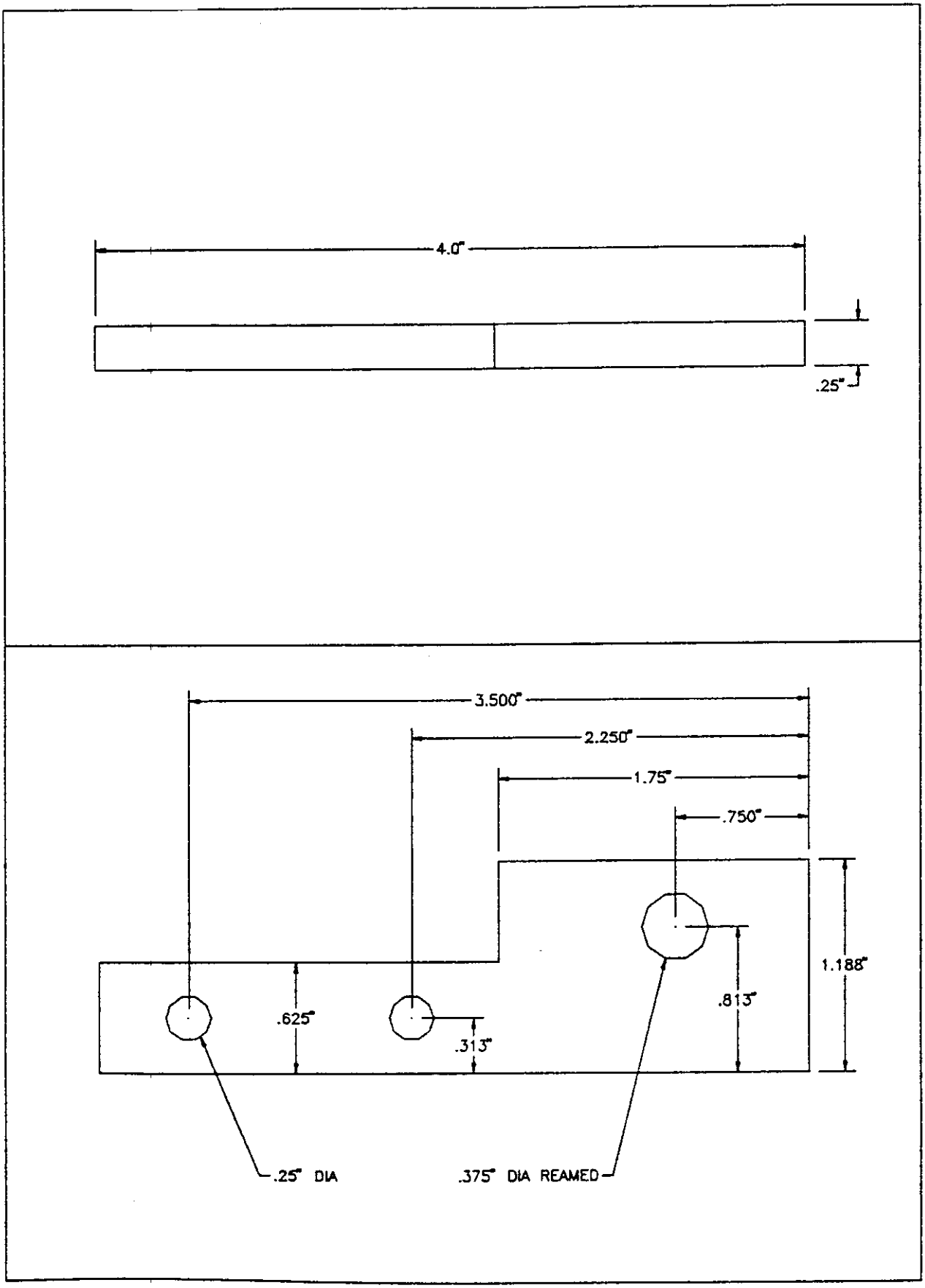

Fig. A-3 Connector

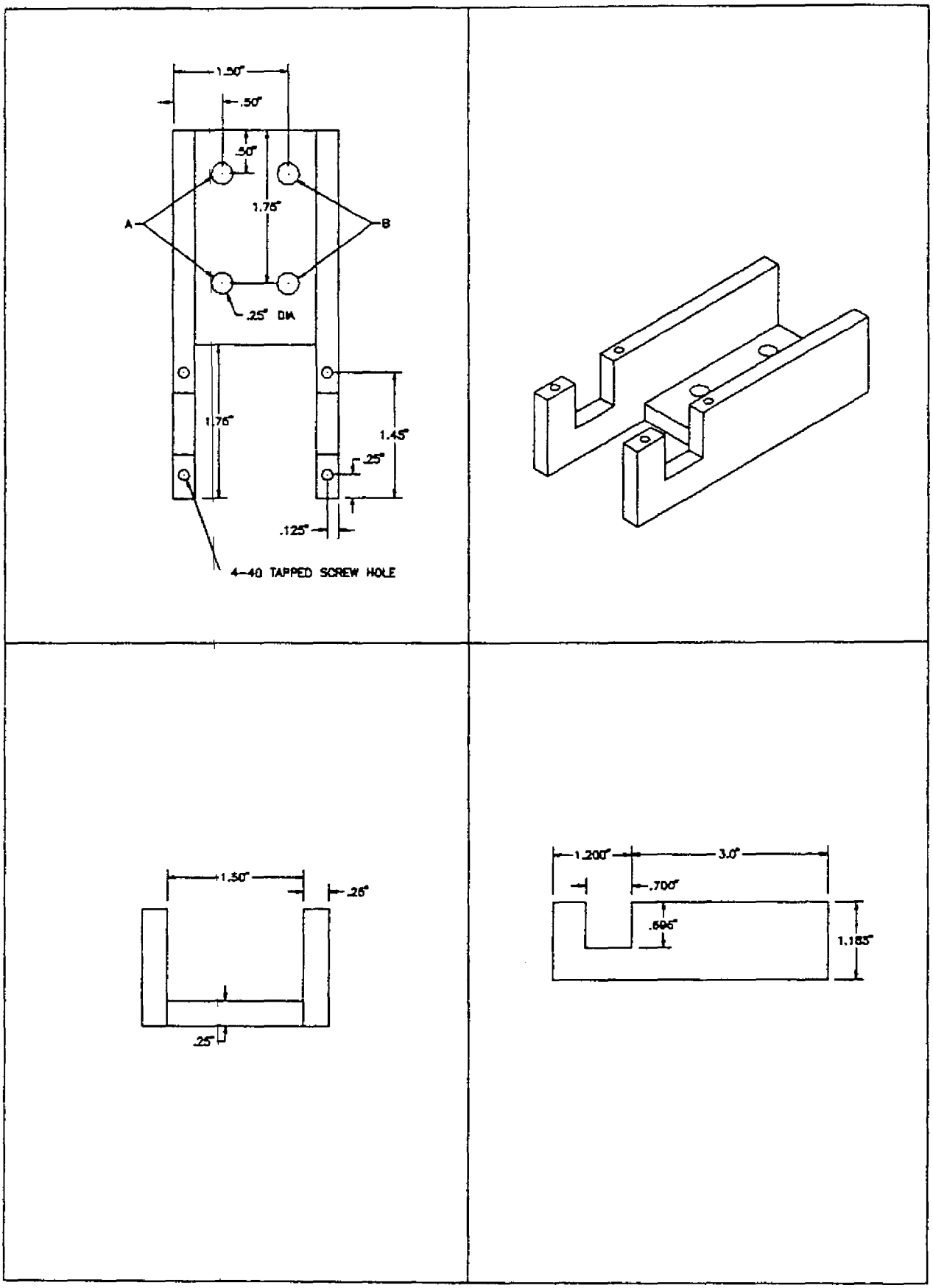

Fig. A-4 Holder

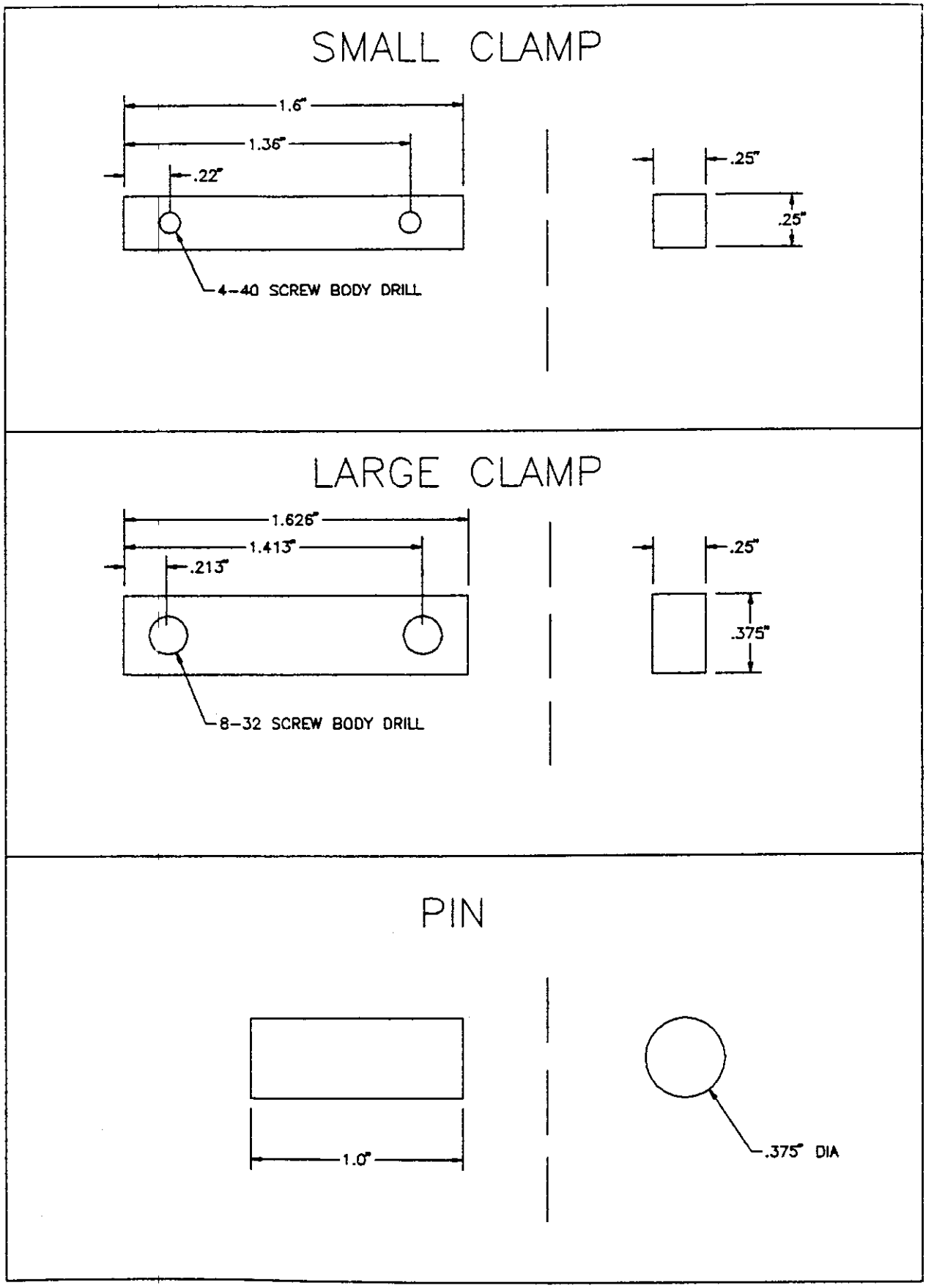

Fig. A-5 Large Clamp, Small Clamp and Pin

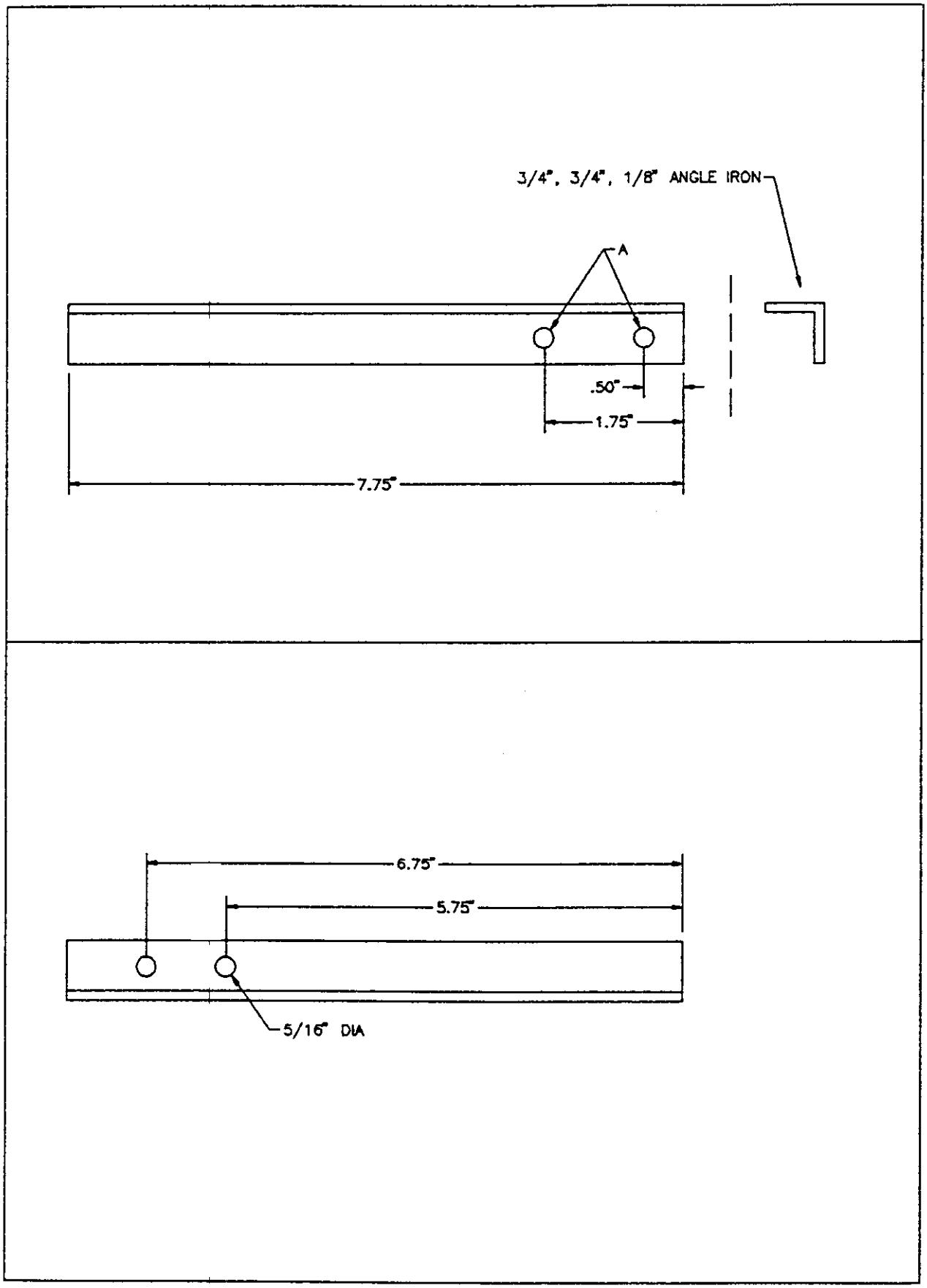

Fig. A-6 Brace A

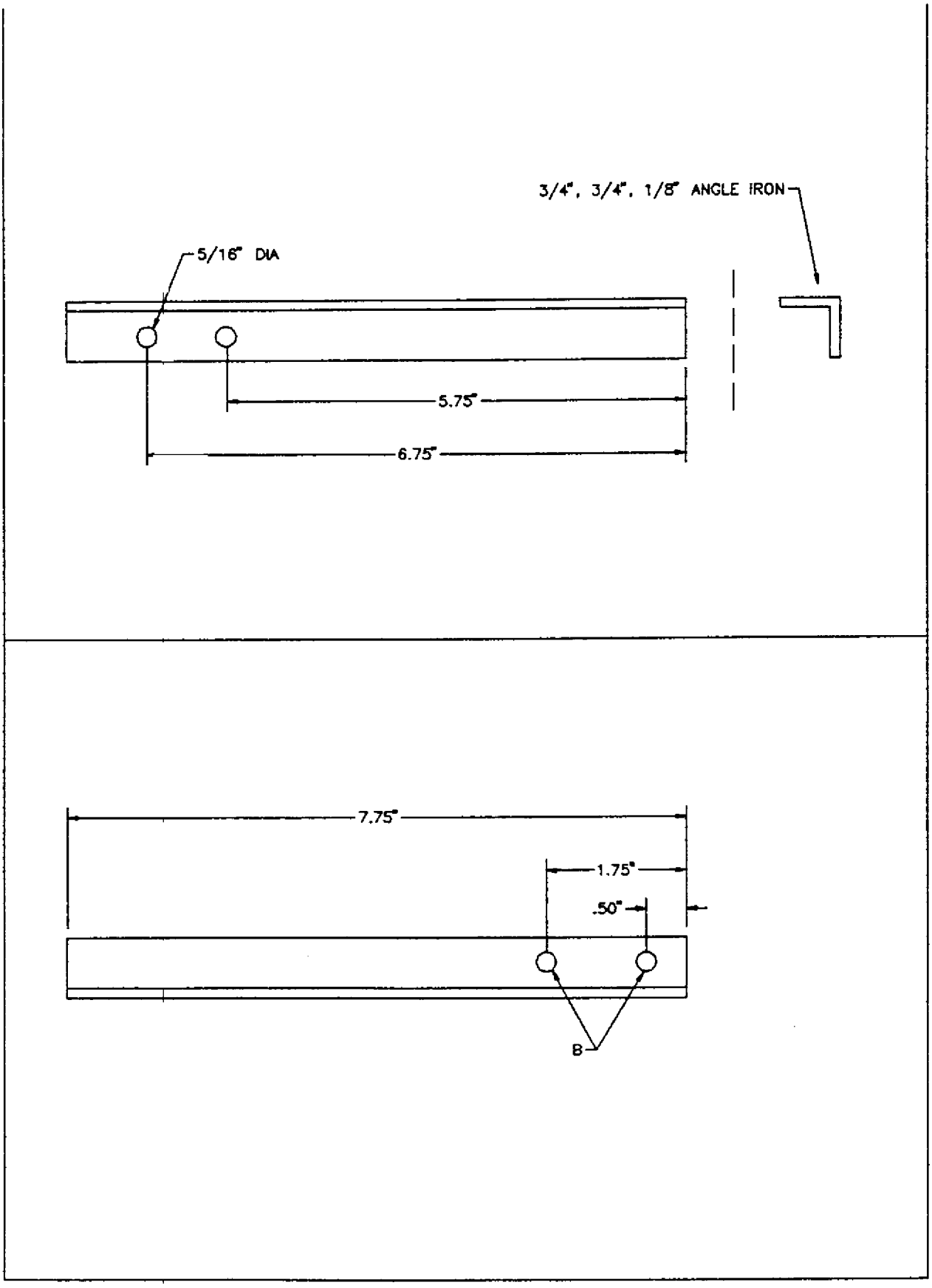

Fig. A-7 Brace B

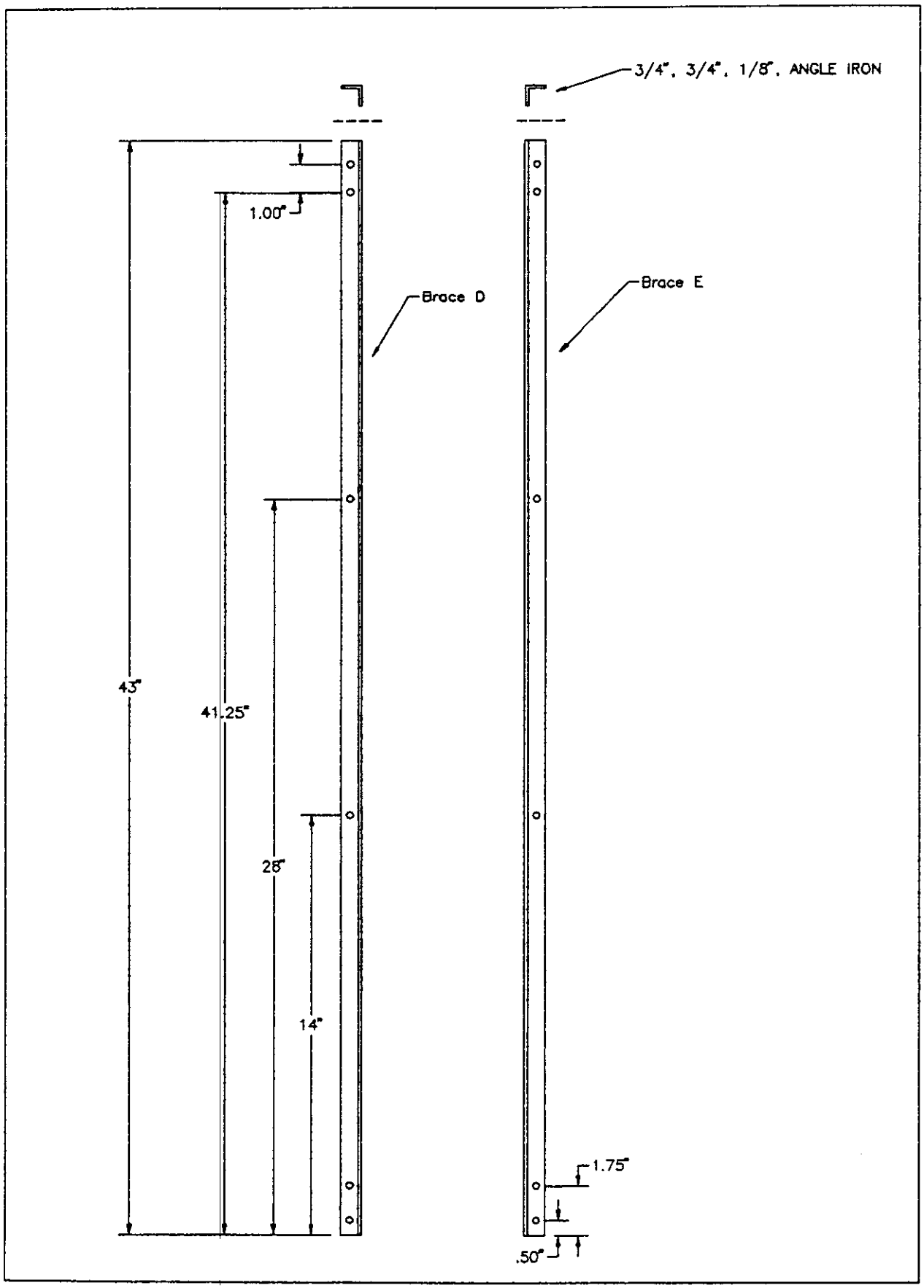

Fig. A-8 Brace D and Brace E

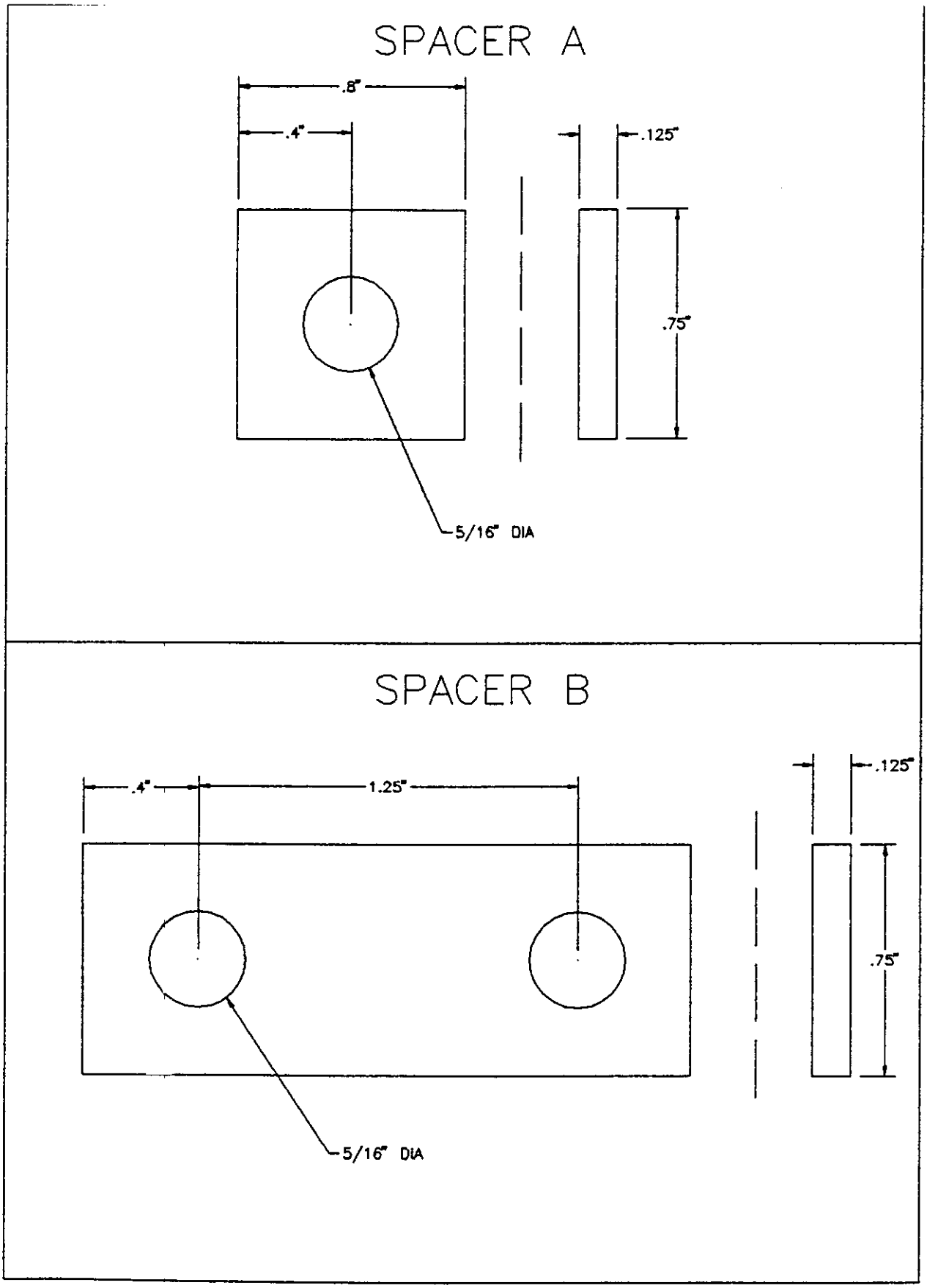

Fig. A-9 Spacers